Multiplicity distributions in high-energy hadron-nucleus collisions. II. Phenomenology

Xin-nian Wang and Rudolph C. Hwa
Institute of Theoretical Science and Department of Physics, University of Oregon, Eugene, Oregon 97403
(Received 21 October 1988)

The calculated results of our formalism for multiplicity distribution in hadron-nucleus collisions are demonstrated and compared with experimental data. The leading particles are found to be responsible for the energy dependence of multiplicity distributions both in hN and hA cases. For shower particles in hA, the Koba-Nielsen-Olesen (KNO) scaling is approximately valid only when the nucleus is heavy but its universality breaks down. The peak of the KNO distribution shifts to smaller values of $n_s/\langle n_s\rangle_{hA}$ when A increases. We also calculate fluctuations of various types. The advantages of measuring the gray-particle multiplicity N_g are discussed. Because of the fluctuation in the number of collisions, there should be no universal behavior for the multiplicity distribution at various impact parameters. Without any free parameter, all the results agree extremely well with experiments.

I. INTRODUCTION

In this second paper of a series of two we shall use the formalism developed in Ref. 1 to investigate the fluctuation in multiplicity. We shall present our predictions on the energy and A dependence of multiplicity distribution in high-energy hadron-nucleus collisions and compare with experimental data.

In the preceding paper[1] we formulate the problem of both hN and hA collisions in terms of effective multiple scatterings and Furry branching process.[2] The common nature of the soft interaction in hN and hA collisions enables us on one hand to have a parameter-free description for the particle-productivity function in hN case,[3] and determine on the other hand the particle-production-related parameter α in hA collisions. The average multiplicity derived, which is a phenomenologically familiar formula, fits the experiments very well without any free parameter for different projectile, target, and incident energies from around 100 GeV. As in hN collisions,[4] the geometrical branching is also the crux of particle production in our formalism for multiplicity distribution in hA collisions in which the geometrical effect is even more enhanced than in the hN case because of the large size of nucleus. As a result, the particle production and the fluctuation in hA collisions should very from one impact parameter and another and on the average should depend on the size or the mass number A of the nucleus. Together with the effects of multiple collision, it is one of the major results we are going to demonstrate in this paper.

Since our formalism is based on the Gribov-Glauber theory of multiple collision, we shall further investigate the fluctuations in the number of collisions ν and multiplicities on a very general ground that the two are closely related. An immediate benefit is the recognition that the detection of the number of gray particles N_g is a superb way to specify the impact parameter of an hA collision. The agreement between our calculation and experimental data on the multiplicity distribution of shower particles for various values of N_g indicates that a universal Koba-Nielsen-Olesen (KNO) scaling cannot exist for each N_g therefore at each impact parameter b, contrary to the assumption made in the other model.[5] We shall also study the energy dependence of the multiplicity distribution and see whether the KNO scaling is violated for a fixed target which is certainly true in the inelastic pp collisions.[6,7] We shall show that the KNO scaling is approximately valid especially for a heavy nucleus, but its universality breaks down due to the A dependence of the multiplicity distribution similar to the N_g or b dependence for a fixed nucleus. The peak of the KNO distribution of shower particles is found to shift to smaller values of $z_{hA}^{(s)}=n_s/\langle n_s\rangle_{hA}$ for heavier nuclei. All of these properties agree well with experimental data available. It is one of the advantages of our formalism that we shall also be able to explain both the physical and mathematical origins of these properties.

Since the hadronic interaction we are considering here is short ranged, the presence of the other nucleons should not affect the first inelastic scattering that h has with a target nucleon in a hA collision. Therefore, when going to the extreme case that A is a nucleon, our formalism should also give the correct results for hN collisions. The energy dependence of multiplicity distribution in the inelastic hN collisions that we get in the following indeed agrees well with experiments. One can consider it as an immediate support that our formalism is realistic and manifests the universality of the particle production in hN and hA collisions. On the other hand it is also an important and fundamental connection that ensures the success of our model in hadron-nucleus collisions.

We shall not repeat all the relevant equations unless necessary since most of the formalism has already been derived in detail in Ref. 1. In the following we shall refer to the equations in Ref. 1 with the prefix I. We only briefly demonstrate how to calculate the moments of the multiplicity distribution in Sec. I and put the detailed derivation in Appendix A.

II. FLUCTUATIONS

Before we present our results on the multiplicity distributions, we give here first some selected features that can provide an insight not only to our model in particular, but also to some characteristics about hA collisions in general. Those features pertain to the fluctuations in ν and n. It is instructive to consider all three forms of $\bar{\nu}$: $\bar{\nu}(b)$, $\bar{\nu}(N_g)$, and $\langle\nu\rangle$. The latter two are measurable, but the first one is of greater theoretical interest because of its specification of b. There has been a long-standing attempt to isolate the value of b by experimental means. Our result should shed some quantitative light on such efforts.

A. Fluctuation in ν

Consider first the fluctuations in ν holding b fixed. We define

$$\overline{\nu^r}(b)\equiv G^{-1}(b)\sum_{\nu=1}^{\infty}\nu^r\pi_\nu(b)\ . \tag{2.1}$$

It follows directly from (I2.7) that

$$\overline{\nu(\nu-1)\cdots(\nu-m)}(b)=G^{-1}(b)[\sigma_{\rm in}^{hN}T(b)]^{m+1}\ . \tag{2.2}$$

Similarly, we have, for fixed N_g,

$$\overline{\nu^r}(N_g)\equiv\sum_{\nu=1}^{\infty}\nu^rP(\nu,N_g)\Big/\sum_{\nu=1}^{\infty}P(\nu,N_g)\ , \tag{2.3}$$

and, for the overall average,

$$\langle\nu^r\rangle\equiv\sum_{\nu=1}^{\infty}\nu^r\sigma_\nu\Big/\sum_{\nu=1}^{\infty}\sigma_\nu\ , \tag{2.4}$$

$$\langle\nu(\nu-1)\cdots(\nu-m)\rangle=\int d^2b[\sigma_{\rm in}^{hN}T(b)]^{m+1}/\sigma_{\rm in}^{hA}\ . \tag{2.5}$$

From these equations we can calculate

$$D_2(\tilde{\nu})\equiv(\tilde{\nu^2}-\tilde{\nu}^2)^{1/2}\ , \tag{2.6}$$

$$D_3(\tilde{\nu})\equiv(\tilde{\nu^3}-\tilde{\nu}^3)^{1/3}\ , \tag{2.7}$$

where $\tilde{\nu^r}$ stands for $\overline{\nu^r}(b)$, $\overline{\nu^r}(N_g)$, or $\langle\nu^r\rangle$. In the calculation for $\overline{\nu^r}(N_g)$, we assume, for illustrative purpose, $\langle N_g\rangle=3.39$ which is an experimental number for ^{197}Au (Ref. 8). For $\langle\nu^r\rangle$ the value of A is to be varied. The results for $D_2(\tilde{\nu})$ and $D_3(\tilde{\nu})$ plotted against the corresponding values of $\tilde{\nu}$ for all three cases are shown in Fig. 1. The solid curves are for $\langle\nu\rangle$. The break in the thickness of the lines at $\langle\nu\rangle=4.11$ indicates that the experimentally accessible range of $\langle\nu\rangle$ is represented by the thick portion (for $A\le238$) and that the theoretical extrapolation to hypothetically larger nuclei is represented by the thin portion. In contrast, even the experimental values of $\bar{\nu}(N_g)$ can reach at least twice the range of $\langle\nu\rangle$. For $\bar{\nu}(b)$ there is a theoretical upper limit for a fixed value of A. It is evident from Fig. 1 that $D_2(\langle\nu\rangle)$ and $D_3(\langle\nu\rangle)$ increase almost linearly with $\langle\nu\rangle$, approximately as

$$D_2(\langle\nu\rangle)\simeq0.58D_3(\langle\nu\rangle)\simeq0.67\langle\nu\rangle\ . \tag{2.8}$$

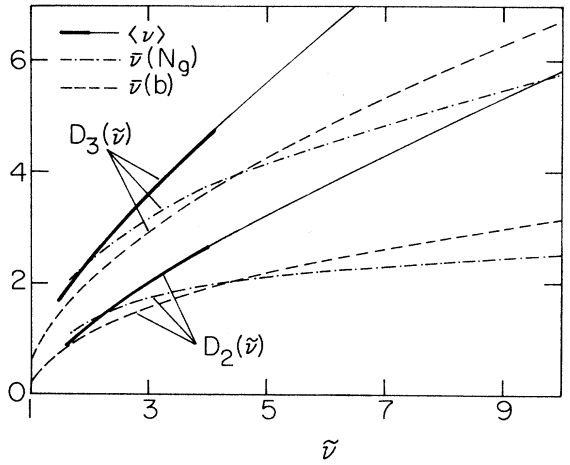

FIG. 1. Fluctuation $D_2(\tilde{\nu})\equiv(\tilde{\nu^2}-\tilde{\nu}^2)^{1/2}$ and $D_3(\tilde{\nu})\equiv(\tilde{\nu^3}-\tilde{\nu}^3)^{1/3}$ of the number of collisions as functions of $\tilde{\nu}$ for three types of averaging corresponding to $\tilde{\nu}=\langle\nu\rangle$ (solid lines), $\bar{\nu}(N_g)$ (dot-dashed lines), and $\bar{\nu}(b)$ (dashed lines). The thick portion of the solid line represents expermentally the accessible range of $\langle\nu\rangle$ up to 4.11 for ^{238}U. The dot-dashed lines are calculated for ^{197}Au with $\langle N_g\rangle=3.39$ (Ref. 8).

But for the other two cases they vary as $(\tilde{\nu})^{1/2}$ for $\tilde{\nu}>3$:

$$D_2(\tilde{\nu})\simeq0.5D_3(\tilde{\nu})\simeq0.94\tilde{\nu}^{1/2}\ , \tag{2.9}$$

where $\tilde{\nu}=\bar{\nu}(b)$ or $\bar{\nu}(N_g)$. For small $\tilde{\nu}$ all three cases are about the same.

Because of the difference between (2.8) and (2.9) and, more importantly, because of the similarity between the two cases where either b or N_g are varied, $\bar{\nu}(N_g)$ is clearly a better experimental variable to choose to describe hA collisions. Compared to $\langle\nu\rangle$, it has a wider range of values, has smaller fluctuations from the mean, and approximates very well the properties associated with holding b fixed. This last feature provides an important connection between experiment and theory. These characteristics will become even more apparent, as we consider the fluctuation in the multiplicity of shower particles.

B. Fluctuation in multiplicities

We consider now the fluctuation in the multiplicity of produced particles. For the normalized moments,

$$C_r=\langle n^r\rangle/\langle n\rangle^r\ , \tag{2.10}$$

it is not necessary to first know the whole multiplicity distribution. That is by virtue of the Furry distribution (I3.3), which satisfies the property[9]

$$\sum_{N=k}^{\infty}\frac{\Gamma(N+m)}{\Gamma(N)}F_N^k(w)=\frac{\Gamma(k+m)}{\Gamma(k)}w^m\ . \tag{2.11}$$

Thus for $m=2$ we have

$$\overline{N^2}=\bar{N}^2+(w-1)\bar{N}=\alpha\nu'(\alpha\nu'+a)\langle n\rangle_{hN}^2\ , \tag{2.12}$$

where (I3.5) and (I3.8) have been used. Now, it follows from (I3.9) that

$$\overline{n^r}(\nu')=\sum_n n^r Q_n(\nu')=\sum_{j=0}^{r}\binom{r}{j}\langle n^i\rangle_{hN}\overline{N^{r-j}}\ , \tag{2.13}$$

where $\langle n^r\rangle_{hN}$ is the average over the hN distribution, $P^{hN}_{n_0}$. Combining (2.12) and (2.13) yields, for $r=2$,

$$\overline{n^2}(\nu')=\langle n\rangle^2_{hN}[C_2^{hN}+(2+\alpha+a)\alpha\nu'+\alpha^2\nu'(\nu'-1)]\ , \tag{2.14}$$

where we have used

$$C_r^{hN}\equiv\langle n^r\rangle_{hN}/\langle n\rangle^r_{hN} \tag{2.15}$$

to denote the moments of the multiplicity distribution of the *produced* particles in the hN collisions. Finally, in averaging over ν', we see from (I2.20) and (I2.21) that the relevant distribution in (I3.11) and (I3.12) is the binomial distribution $B_{\nu'}(\nu-1,p)$, which possesses the property

$$\sum_{\nu'=0}^{\nu-1}\frac{\nu'!}{(\nu'-m)!}B_{\nu'}(\nu-1,p)=\frac{(\nu-1)!p^m}{(\nu-m-1)!}\ . \tag{2.16}$$

Thus, we obtain, from (I3.11), (I3.12), (I1.13), and (2.16),

$$\langle n^2\rangle_{hA}(\tilde\nu)=\langle n\rangle^2_{hN}[C_2^{hN}+(2+\alpha+a-2\beta)\beta(\tilde\nu-1)+\beta^2\langle\nu(\nu-1)\rangle^{\sim}]\ , \tag{2.17}$$

where $\beta=\alpha p$. In (2.17), $\langle\cdots\rangle^{\sim}$ denotes the averages of types (2.1), (2.3), or (2.4) according to what $\tilde\nu$ is. Then for $\tilde\nu=\bar\nu(b)$, $\overline{\nu(\nu-1)}(b)$ is given by (2.2); for $\bar\nu(N_g)$, $\overline{\nu^r}(N_g)$ is given by (2.3); finally, for $\langle\nu\rangle$, $\langle\nu(\nu-1)\rangle$ is given by (2.5). Note how $\langle n^2\rangle_{hA}(\tilde\nu)$ is influenced by the fluctuation in ν, i.e., $\tilde\nu^2$.

The last step is the conversion to the multiplicity of the shower particles, which is what is measured. From (I5.2) we have

$$\overline{n_s^r}(\nu')=\sum_{n_s}n_s^r Q^s_{n_s}(\nu')=\sum_{i=0}^{r}\binom{r}{i}\overline{(m+1)^i}(\nu')\overline{n^{r-i}}(\nu')\ , \tag{2.18}$$

where $\overline{n^{r-i}}(\nu')$ is given by (2.13) and

$$\overline{(m+1)^i}(\nu')\equiv\sum_{m=0}^{\nu'}(m+1)^i B_m(\nu',q)\ . \tag{2.19}$$

Note that, for $r=1$, we have

$$\overline{n_s}(\nu')=1+q\nu'+\bar n(\nu')\ , \tag{2.20}$$

which, by virtue of (I3.10) and (2.16), yields (I5.1). For $r=2$ we have

$$\overline{n_s^2}(\nu')=1+3q\nu'+q^2\nu'(\nu'-1)+\overline{n^2}(\nu')+2\langle n\rangle_{hN}[1+(q+\alpha+\alpha q)\nu'+\alpha q\nu'(\nu'-1)]\ . \tag{2.21}$$

Using (2.16) and then (I3.11), (I3.12), and (I3.13) we obtain

$$\langle n_s^2\rangle_{hA}(\tilde\nu)=1+2\langle n\rangle_{hA}(\tilde\nu)+(\tilde\nu-1)pq[3-2pq+2(1+\alpha-2\beta)\langle n\rangle_{hN}]+(\tilde\nu^2-\tilde\nu)pq(pq+2\beta\langle n\rangle_{hN})+\langle n^2\rangle_{hA}(\tilde\nu)\ . \tag{2.22}$$

The determination of $\langle n_s^3\rangle_{hA}(\tilde\nu)$ is similar but more tedious. It is given in the Appendix.

With these results we now construct the normalized moments:

$$C_r^{(s)}=\langle n_s^r\rangle_{hA}/\langle n_s\rangle^r_{hA}\ . \tag{2.23}$$

In calculating these moments we need C_r^{hN} and the parameter a defined in (I3.5), as is evident in (2.17), (A19), and (A20). It should be stressed that C_r^{hN} do not correspond to the moments of the KNO scaling curve in non-single-diffractive (NSD) events. The reason is that, as defined in (2.15), they are the moments of the multiplicity distribution that includes only produced charged particles from all inelastic events, not just those arising from NSD reactions. It is the latter that exhibit KNO scaling for $\sqrt{s}<100$ GeV (or $E_{\rm lab}<10^4$ GeV). When all inelastic events are considered, including the single-diffractive (SD) ones, the multiplicity distribution does not have the scaling property any more even in the same energy range.[6,7] This may be attributed to the fact that the leading particles in the SD events are not negligible among the produced particles which are quite fewer than in NSD events. It is conjectured[10,11] that only the produced particles in inelastic pp collisions obey KNO scaling. Evidently, the SD events decrease the average multiplicity and thus increase the fluctuation or the moments $C_r^{hN}=\langle n^r\rangle_{hN}/\langle n\rangle^r_{hN}$. When the leading particles are included, the resultant multiplicity distribution will depend on the energy. The calculation of parameter a and moments C_r^{hN}, $r\geq 3$, is done in the next section with an input of $C_2^{hN}=1.32\pm0.01$, which can be extracted from experiments when we consider the energy dependence of the dispersion of multiplicity distribution in pp collisions. The moments are approximately scaling quantities having the values $C_3^{hN}=2.13\pm0.05$, and a is found to have the value of 0.23 ± 0.01. We use them in our determination of $C_2^{(s)}$ and $C_3^{(s)}$. The dispersion and skewness defined by

$$D^{(s)}=[\langle(n_s-\langle n_s\rangle_{hA})^2\rangle]^{1/2}\ , \tag{2.24}$$

$$S^{(s)}=[\langle(n_s-\langle n_s\rangle_{hA})^3\rangle]^{1/3}\ , \tag{2.25}$$

can be expressed in terms of $C_r^{(s)}$ by

$$D^{(s)}/\langle n_s\rangle_{hA}=(C_2^{(s)}-1)^{1/2}\ , \tag{2.26}$$

$$S^{(s)}/\langle n_s\rangle_{hA}=(C_3^{(s)}-3C_2^{(s)}+2)^{1/3}\ . \tag{2.27}$$

These two quantities are plotted versus $\tilde\nu$ in Figs. 2 and 3 for the three cases of $\tilde\nu$. The lines have the same representational meanings as in Fig. 1. Notice that while the dispersion and skewness stay high for $\tilde\nu=\langle\nu\rangle$, especially in the physical region (thick solid lines), they decrease

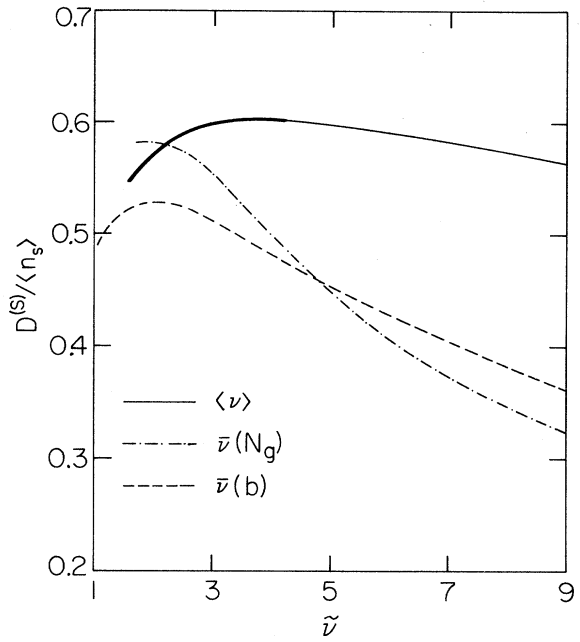

FIG. 2. The normalized dispersion of shower particles in hA collisions as functions of $\tilde{\nu}$. The lines have the same meaning as in Fig. 1.

significantly as $\bar{\nu}(b)$ and $\bar{\nu}(N_g)$ increase. This phenomenon is anticipated as a consequence of the lower fluctuation in ν for the latter two cases, as revealed in Fig. 1. The similarity between the dashed and dash-dot curves in Figs. 2 and 3 is the basis of our assertion that a measurement of the multiplicity distribution for various fixed N_g values is tantamount to measuring the multiplicity distribution for various fixed impact parameter b. This establishes a significant bridge between experiment and theory.

Finally, to verify our predictions on the fluctuation in multiplicities, we compare the calculated results with the experimental data[12] of pXe collisions in Fig. 4 for the case of $\tilde{\nu}=\bar{\nu}(N_g)$. We defer the comparison for the case of $\tilde{\nu}=\langle \nu \rangle$ until we discuss the A dependence of the multiplicity distribution. The agreement between our calculation and the data in Fig. 4 is evidently very good. To exhibit the dependences on the target nucleus, the same plot is made in Fig. 5 for proton on ^{197}Au (solid line) and ^{24}Mg (dashed line). We see that $D^{(s)}/\langle n_s \rangle_{hA}$ depends only slightly on A compared with the dependence on $\bar{\nu}(N_g)$. At the peak where the value of $D^{(s)}/\langle n_s \rangle_{hA}$ for $\bar{\nu}(N_g)$ roughly agrees with that for $\langle \nu \rangle$ (see Fig. 2), they are not too far off from the corresponding value for pp (indicated by the dash-dot line in Fig. 5).

An important feature to notice is that Figs. 4 and 5 clearly reveal a strong dependence of $D^{(s)}/\langle n_s \rangle_{hA}$ on $\bar{\nu}(Ng)$, and by virtue of Fig. 2 therefore also on $\bar{\nu}(b)$. It means that the fluctuation of the multiplicity distribution at various b values are not the same. The assumption of a constant KNO scaling curve for all b is therefore untenable, contrary to the assumption made in other approaches to the problem.[5] Our result indicates that $C_2(b)$ decreases with decreasing b. The origin of this behavior can be traced to (I3.11) where, if $Q_n(\nu')$ were to give a $C_2(\nu')$ that is approximately constant for a fixed value of ν', it is $\prod_{\nu,\nu'}(b)$ which effects a fluctuation in ν' or ν at each fixed b. Because of (2.9) we have $D_2(\tilde{\nu})/\tilde{\nu} \sim (\tilde{\nu})^{-1/2}$, thus causing the normalized dispersion to decrease with increasing $\tilde{\nu}$, or decreasing b. From (I3.17) and (2.17) it is quite evident that $C_2^{(s)}$ at fixed b is strongly dependent on the dispersion for $\bar{\nu}(b)$, i.e., on $D_2\ (\bar{\nu}(b))/\bar{\nu}(b)$. That dependence results in the decrease of $C_2^{(s)}$ with decreasing b.

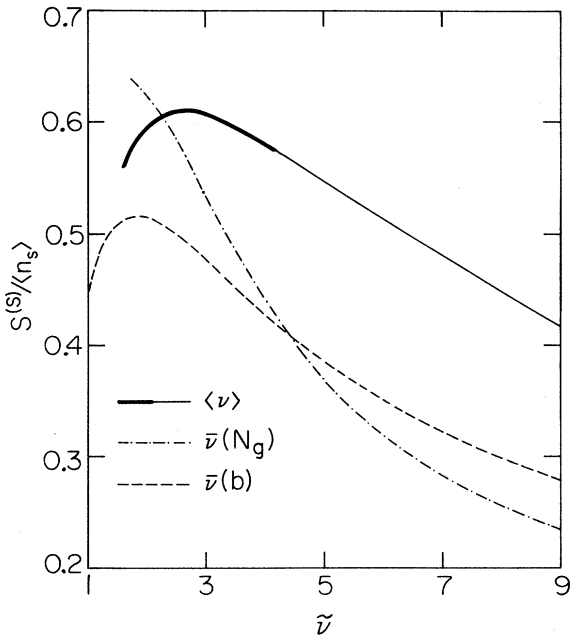

FIG. 3. The normalized skewness of shower particles in hA collisions as functions of $\tilde{\nu}$. The lines have the same meaning as in Fig. 1.

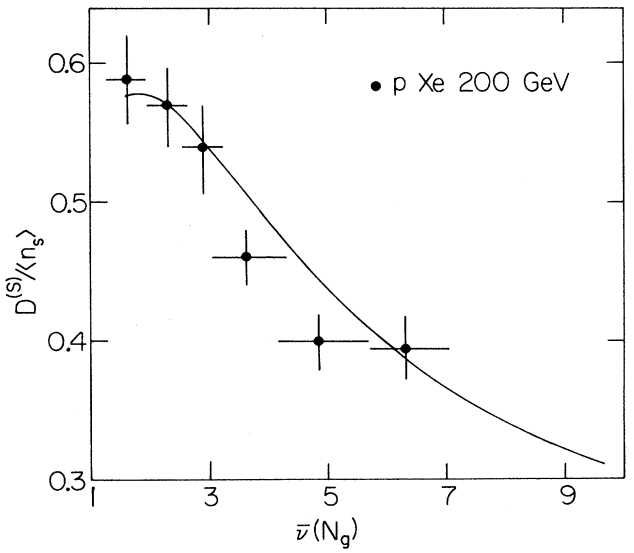

FIG. 4. The normalized dispersion of shower particles in pXe collisions as a function of $\bar{\nu}(N_g)$. The data are from Ref. 12. The line is the theoretical result in the paper.

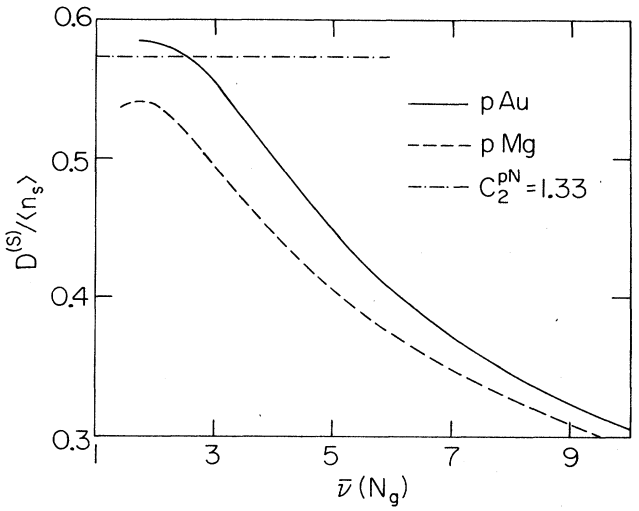

FIG. 5. The normalized dispersion of shower particles in pAu (solid line) and pMg (dashed line) collisions as functions of $\bar{\nu}(N_g)$. The dot-dashed line indicate the normalized dispersion of produced particles in hN collisions.

III. ENERGY DEPENDENCE OF MULTIPLICITY DISTRIBUTIONS

For only produced particles in hA collisions, the moments of multiplicity distribution given in (A18)–(A20) are almost independent of energy similar to the case of hN. This is due to the particular property of Furry distribution which is approximately KNO scaling after smeared over impact parameter. Therefore we shall only discuss the energy dependence of the multiplicity distribution of shower particles. Since the similarity between hN and hA interactions requires that our general formalism in Ref. 1 should also give a good description for the multiplicity distribution in hN collisions, we have to check the results for hN before we go to the case of hA collisions. But first of all it is necessary to summarize our definition of charged leading, produced, and shower particles as stated scrappily in Ref. 1.

In an NN collision, we call the nucleons in the fragmentation region in the c.m. system as leading particles. The average charged leading particles is then 1 due to the processes such as $p\to\pi^0 p$, $\pi^- n$ and $n\to\pi^0 n$, $\pi^- p$. The produced and shower particles exclude and include these leading particles, respectively. We thus have, from (I3.22) and (I5.1),

$$\langle n_s\rangle_{hA}=1+\gamma(\langle\nu\rangle-1)+\langle n\rangle_{hN}[1+\beta(\langle\nu\rangle-1)]\ , \tag{3.1}$$

where $\gamma=qp$ and $\langle n\rangle_{hN}$ is the average number of produced charged particles in an hN collision. The scaling form of multiplicity distribution for an hN collision,

$$\psi_{hN}(z_{hN})=\langle n\rangle_{hN}P_n^{hN}(\langle n\rangle_{hN})\ ,\qquad z_{hN}=n/\langle n\rangle_{hN}\ , \tag{3.2}$$

is only for the produced particles, which should be the one for the first inelastic hN collision in an hA collision. P_n^{hN} in (3.2) is given by (I4.12),

$$P_n^{hN}(\langle n\rangle_{hN})=\int_0^\infty dR^2 g(R)F_n^{k(R)}(w)\equiv\{F_n^{k(R)}\}\ , \tag{3.3}$$

with the initial number of clusters at R:

$$k(R)\equiv\langle k\rangle_{hN}h(R)=\langle k\rangle_{hN}\frac{\Omega(R)}{(1-e^{-2\Omega(R)})\int_0^\infty dR^2\Omega(R)}\ , \tag{3.4}$$

where

$$\{\cdots\}=\int_0^\infty dR^2 g(R)(\cdots)=\int_0^\infty dR^2(1-e^{-2\Omega(R)})(\cdots)\ , \tag{3.5}$$

$F_n^{k(R)}(w)$ is the Furry distribution with $w=\langle n\rangle_{hN}/\langle k\rangle_{hN}$ and $\langle k\rangle_{hN}=\{k\}$ is the average total number of initial clusters in a pp collision. The distribution in (3.3) is exactly the multiplicity distribution obtained in the geometrical branching model[4] (GBM) which describes the KNO scaling of the multiplicity distribution in non-single-diffractive pp collisions very well for $E_{\rm lab}<10^4$ GeV. We shall show in this section that (3.3) also works for the produced charged particles in inelastic pp collisions.

A. The case for hN collisions

We can extract the result for hN collisions from the formalism in Ref. 1 simply by setting the number ν of hN scatterings to 1 and assuming no fluctuation in ν, i.e., $\langle\nu^r\rangle=1$. Thus we have, from (3.1),

$$\langle n_s\rangle_{hN}=1+\langle n\rangle_{hN}\ , \tag{3.6}$$

which is just the definition of average produced particles $\langle n\rangle_{hN}$ in (I5.4). For the consistency of our formalism, we still keep the subscript (or superscript) s for total charged particles in hN collisions to distinguish them from the produced ones although s here has lost its original meaning of shower particles in the case of hA collisions. For the multiplicity distribution of total charged particles in hN collisions we have, by (I3.9) and (I5.2),

$$\mathcal{P}^s_{n_s}=P^{hN}_{n_s-1}(\langle n\rangle_{hN})\ , \tag{3.7}$$

where $P_n^{hN}(\langle n\rangle_{hN})$ is given by (3.3). From (A22)–(A28) or calculating directly by (3.7) we have

$$\langle n_s^2\rangle_{hN}=1+2\langle n\rangle_{hN}+C_2^{hN}\langle n\rangle_{hN}^2\ , \tag{3.8}$$

$$\langle n_s^3\rangle_{hN}=1+3\langle n\rangle_{hN}+3C_2^{hN}\langle n\rangle_{hN}^2+C_3^{hN}\langle n\rangle_{hN}^3\ . \tag{3.9}$$

Using (3.6) we obtain the dispersion and skewness in terms of the total charged multiplicity $\langle n_s\rangle_{hN}$:

$$D^{(s)}=(\langle n_s\rangle_{hN}-1)(C_2^{hN}-1)^{1/2}\ , \tag{3.10}$$

$$S^{(s)}=(\langle n_s\rangle_{hN}-1)(C_3^{hN}-3C_2^{hN}+2)^{1/3}\ . \tag{3.11}$$

With constant C_2^{hN}, (3.10) gives us the familiar Wrob-

lewski[13] empirical form which has been widely used to fit experimental data.[6,7] The value of C_2^{hN} thus extracted from the comparison of (3.10) with experiments is

$$C_2^{hN}=1.32\pm0.01 \ . \tag{3.12}$$

Following the same procedure as in the NSD case of pp collisions,[4] we have, from (3.3),

$$C_2^{hN}=\{h^2\}+(w-1)/\langle n\rangle_{hN} \ , \tag{3.13}$$

$$C_3^{hN}=\{h^3\}+3[w\{h^2\}-C_2^{hN}]/\langle n\rangle_{hN}+2(w^2-1)/\langle n\rangle_{hN}^2 . \tag{3.14}$$

With the value of C_2^{hN} in (3.12) we have

$$a\equiv(w-1)/\langle n\rangle_{hN}=0.23\pm0.01 \ , \tag{3.15}$$

$$C_3^{hN}=2.16\pm0.05 \ . \tag{3.16}$$

The error in (3.16) comes from that of C_2^{hN} in (3.13) and a slight energy dependence for $E_{\rm lab}\geq 50$ GeV. Knowing C_2^{hN} and C_3^{hN}, we thus can calculate the energy dependence of $S^{(s)}$ from (3.11). In Fig. 6 we show the normalized dispersion and skewness as functions of the incident energy $E_{\rm lab}$. The curves are from (3.10) and (3.11) and the experimental data points are from Refs. 6 and 14. The good agreement between the two is evident. We can see from (3.10) and (3.11) that the energy dependence of the multiplicity distribution $\mathcal{P}^s_{n_s}$ is mainly caused by the presence of leading particles when the produced ones have a scaling distribution. At higher energies more particles are produced, then the leading particles are less important and the multiplicity distribution would tend to the scaling form. But for $E_{\rm lab}\gtrsim 10^4$ GeV, jet production becomes important and it will increase the fluctuation or the moments C_r^{hN} to higher values as it does in the nonsinglet-diffractive events.[15] Further investigation of this effect is beyond the scope of the subject here.

Although (3.10) and (3.11) have been proposed and fitted[10,11] to experiments before, this is the first time GBM is used to derive the scaling multiplicity distribution of produced particles in an inelastic pp collision. The moments C_r^{hN} calculated from GBM give the proper normalizations to make $S^{(s)}$ and higher moments for the total charged particles agree with experiments. Since all the results in this subsection are included in the formalism for pA interaction and the multiplicity distribution in pA collisions in turn depends on that of pN, the success here evidently verifies the foundation of our model and ensures the reliability of our predictions for the energy and A dependence of the multiplicity distribution in hA collisions. Together with the results in Ref. 1, it demonstrates how the particle production in hN and hA are connected and it is the inherent ability of our formalism which can manifest this connection.

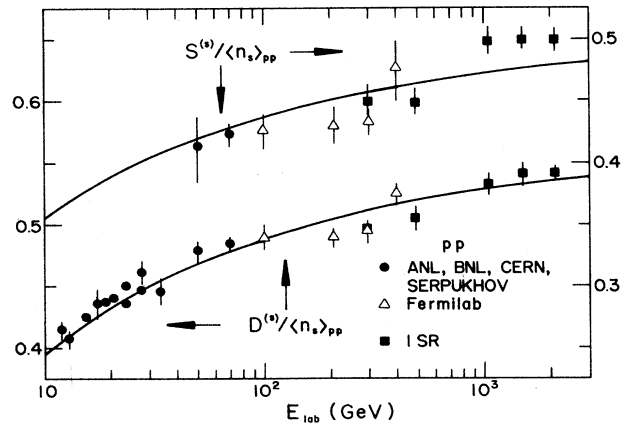

FIG. 6. The energy dependence of the normalized dispersion and skewness of the total charged particles in inelastic pp collisions. The data are from Ref. 6. The curves are the calculated results in the paper. Notice the scale at left for dispersion is different from that at right for skewness.

We now define the KNO distribution for the inelastic hN collisions as

$$\psi^s_{hN}(z^{(s)}_{hN})=\langle n_s\rangle_{hN}\mathcal{P}^s_{n_s} \ , \tag{3.17}$$

where $z^{(s)}_{hN}=n_s/\langle n_s\rangle_{hN}$. By (3.2) and (3.7) we have then

$$\psi^s_{hN}(z^{(s)}_{hN})=\frac{1}{1-1/\langle n_s\rangle_{hN}}\psi_{hN}\left[\frac{z^{(s)}_{hN}-1/\langle n_s\rangle_{hN}}{1-1/\langle n_s\rangle_{hN}}\right] , \tag{3.18}$$

where $\psi_{hN}(z)$ is given by (3.2) and (3.3). From the above equations we can immediately obtain (3.10) and (3.11) by the definitions of $D^{(s)}$ and $S^{(s)}$,

$$D^{2(s)}/\langle n_s\rangle^2_{hN}=\int_0^\infty dz^{(s)}_{hN}(z^{(s)}_{hN}-1)^2\psi^s_{hN}(z^{(s)}_{hN}) \ , \tag{3.19}$$

$$S^{3(s)}/\langle n_s\rangle^3_{hN}=\int_0^\infty dz^{(s)}_{hN}(z^{(s)}_{hN}-1)^3\psi^s_{hN}(z^{(s)}_{hN}) \ . \tag{3.20}$$

B. The case for hA collisions

For hA collisions, the corresponding equations for dispersion and skewness of the multiplicity distributions of shower particles are more complicated than (3.10) and (3.11) for hN collisions. But the energy dependence should also be caused by the leading particles, because the multiplicity distribution of the produced particles is almost independent of energy as in the case of hN. In Figs. 7 and 8 we show the normalized dispersion and skewness of the multiplicity distribution in hA collisions as functions of $E_{\rm lab}$. They are calculated from (A21)–(A28). For comparison we give the results for pAu (solid line) and pC (dashed line) along with results for pp (dot-dashed line). It is clear that the three curves have a similar energy dependence, since they are all induced by the leading particles in the energy range $E_{\rm lab}<10^4$ GeV which we are considering here. For a heavier nucleus the total average produced multiplicity $\langle n\rangle_{hA}$ is larger. So the leading particles are comparatively less important and the therefore the multiplicity distribution is less dependent on energy. We indeed find in Figs. 7 and 8 that $D^{(s)}/\langle n_s\rangle_{hA}$ and $S^{(s)}/\langle n_s\rangle_{hA}$ are almost constant for pAu collision. We may conclude that KNO scaling is approximately valid for hA collisions especially for heavy nuclei. The experimental data which

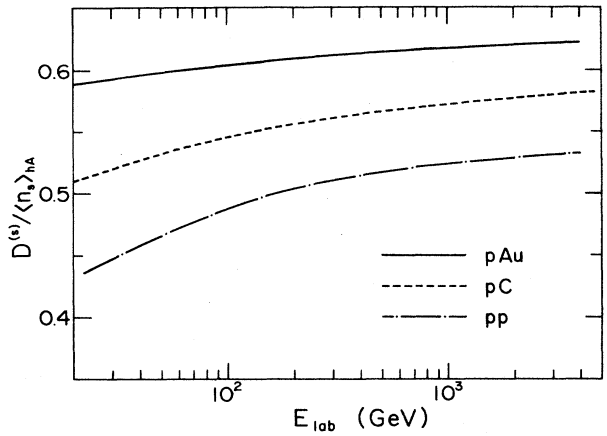

FIG. 7. The prediction for the energy dependence of the normalized dispersion of shower particles in pAu (solid line), pC (dashed line), and pp (dot-dashed line) collisions.

we shall compare with our calculation in the next section at $E_{\rm lab}=100$ GeV and $E_{\rm lab}=200$ GeV do show no difference from each other within the error bars. Unfortunately, we do not have many data to further prove our predictions.

Finally, we must emphasize that the leading particles play an important role in the energy dependence of multiplicity distribution of shower particles (or total charged particles in hN collisions). When we only consider the produced particles, the multiplicity distributions both in hN and hA cases are approximately KNO scaling, because Furry branching is the basic particle production process in both cases and the Furry distribution is approximately KNO scaling after smeared over impact parameter. When energy goes beyond the range relevant here jet production must be very important as has been shown by the increase of the total inelastic cross section of pA collisions.[16,17] As in hadron-hardon collisions,[15] its effect on multiplicity distribution in hA should be prominent.

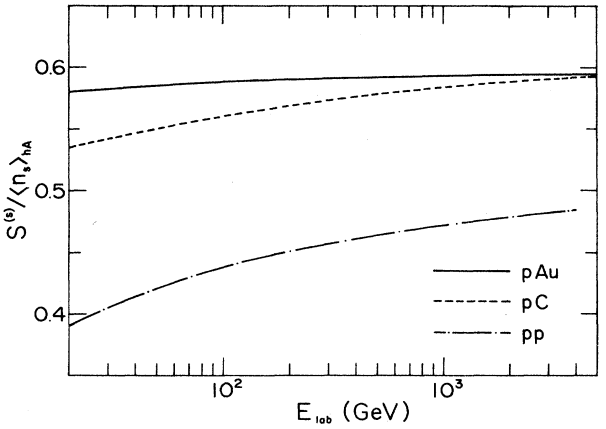

FIG. 8. The prediction for the energy dependence of the normalized skewness of shower particles in pAu (solid line), pC (dashed line), and pp (dot-dashed line) collisions.

IV. A DEPENDENCE OF MULTIPLICITY DISTRIBUTION

In this section we shall study the A dependence of multiplicity distribution. Since the energy dependence is small especially for heavy nuclei, we shall only focus on the predictions at a fixed energy. All the results of our calculation in the following are for $E_{\rm lab}=100$ GeV, and all experimental data which we are comparing with are also in the vicinity of this energy.

A. Moments

In Sec. I we have discussed the fluctuation in multiplicity on a general ground that it is related to the fluctuation in the number of scatterings ν. Among the three cases which we considered, i.e., fixing the impact parameter b, fixing the number N_g of gray particles, and unconditioned (averaging everything), the last one has the largest fluctuation in ν, particularly for heavy nuclei. According to our formalism, the average multiplicity is proportional to ν; therefore, the fluctuation in multiplicity for the unconditioned distribution is also the largest, which is the case we are considering here. Since the average number of scatterings,

$$\langle\nu\rangle = A\sigma_{\rm in}^{hN}/\sigma_{\rm in}^{hA}\ , \tag{4.1}$$

is a monotonic increasing function of the mass number A of the target nucleus for a fixed projectile h, we plot the normalized dispersion and skewness as functions of $\langle\nu\rangle$ in Figs. 9 and 10 to show the A dependence of multiplicity distribution. The curves are calculated from our formalism (A21)–(A28) for pA collisions. We believe that the Wood-Saxon form of nuclear density is not relevant any more for light nuclei. So we only calculated $D^{(s)}$ and $S^{(s)}$ down from a certain nucleus for which we consider the results are still reliable. We take this nucleus to be C

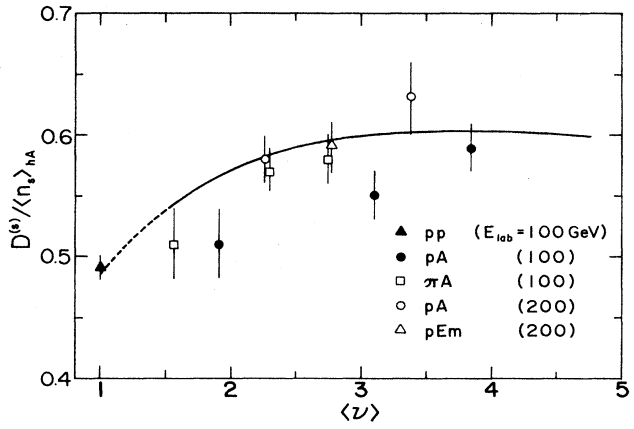

FIG. 9. The normalized dispersion of shower particles in hA collisions as a function of $\langle\nu\rangle$ for various nuclei. The solid line is calculated results with $E_{\rm lab}=100$ GeV. The dashed line is the extrapolation of the solid line to the calculated point for pp collisions. The data are from Ref. 6 (solid triangle), Ref. 8 (solid circle and open square), Ref. 12 (open circle), and Ref. 18 (open triangle).

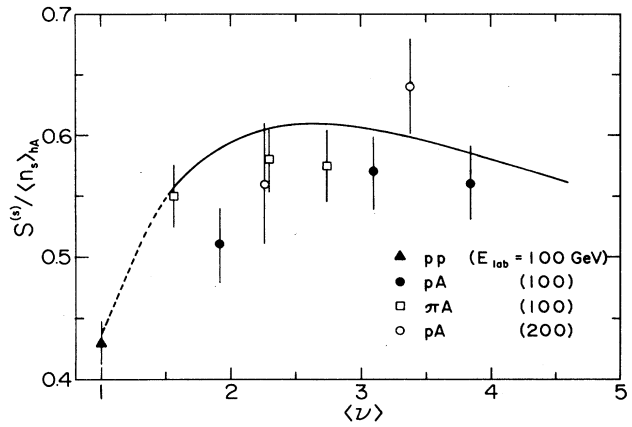

FIG. 10. The normalized skewness of shower particles in hA collisions as a function of $\langle\nu\rangle$ for various nuclei. The lines have the same meaning as in Fig. 9. The data are from Ref. 6 (solid triangle), Ref. 8 (solid circle and open square), and Ref. 12 (open circle).

and show the results as solid lines. We use dashed lines to connect the solid ones with the result for the pp case obtained in the last section. The experimental data are from Refs. 6, 8, 12, and 18. The A dependence of $D^{(s)}/\langle n_s\rangle_{hA}$ and $S^{(s)}/\langle n_s\rangle_{hA}$ is evident and our calculation agrees well with the data as shown in Figs. 9 and 10. Theoretically, as shown in Figs. 2 and 3, both $D^{(s)}/\langle n_s\rangle_{hA}$ and $S^{(s)}/\langle n_s\rangle_{hA}$ would decrease with $\langle\nu\rangle$ or A for hypothetically large nuclei after the initial increase at small $\langle\nu\rangle$ or A. But realistically, $\langle\nu\rangle=4.11$ for pU is the largest value we can get in experiments. So we can only see the increasing part of $D^{(s)}/\langle n_s\rangle_{hA}$ and the beginning of the decrease of $S^{(s)}/\langle n_s\rangle_{hA}$. As this is concerned, we would prefer more experimental data with specified number of gray particles, as shown in Figs. 4 and 5, to testify our formalism of multiplicity distribution in hA collisions, since the experimentally achievable range of $\bar{\nu}(N_g)$ is always more than twice of $\langle\nu\rangle$.

The smooth extrapolation of our calculation for pA to pp collisions shows how the multiplicity distributions in two cases are related. As can be seen from (A21)–(A28) and observed during our calculation, the normalized dispersion $D^{(s)}/\langle n_s\rangle_{hA}$ and skewness $S^{(s)}/\langle n_s\rangle_{hA}$ for each A depend on the values of C_2^{hN}, C_3^{hN} and the parameter $a=C_2^{hN}-\{h^2\}$ which are determined in the GBM of pp collisions (see Sec. II). The good agreement between the calculation and the data in Figs. 9 and 10 once again is another support for our universal treatment to the particle production in pp and pA collisions, thus for the idea that parton interaction underlies the physics for both pp, pA, and AA collisions.

In Figs. 9 and 10 we also give the experimental data for πA which does not show much difference from pA collisions. Our calculation gives the same result if we assume that the multiplicity distributions for πN and NN are the same. Until the multiplicity distribution for πN collisions is investigated, we do not have any comments on this problem. But recalling the good fitting of the average produced multiplicity (I3.22) to both the experimental data of pA and πA, we believe that the two should not be very different.

B. The KNO distribution

The KNO distribution of the shower particles in hA collisions is defined as

$$\psi_{hA}^{s}(z_{hA}^{(s)})=\langle n_s\rangle_{hA}\mathcal{P}_{n_s}^{s}\ , \tag{4.2}$$

where $z_{hA}^{(s)}=n_s/\langle n_s\rangle_{hA}$. $\mathcal{P}_{n_s}^{s}$ is the corresponding multiplicity distribution which can be formulated in terms of multiple scattering probability [see (I3.13) and (I5.2)]. We only outline the formula for $\mathcal{P}_{n_s}^{s}$ here and refer readers to Ref. 1 for detailed discussion. Let us rewrite it as

$$\mathcal{P}_{n_s}^{s}=(\sigma_{\rm in}^{hA})^{-1}\int d^2b\sum_{\nu=1}^{\infty}\sum_{\nu'=0}^{\nu-1}\Pi_{\nu,\nu'}(b)Q_{n_s}^{s}(\nu')$$
$$\equiv\sum_{\nu=1}^{\infty}P_{n_s}^{s}(\nu)\ , \tag{4.3}$$

so that $P_{n_s}^{s}(\nu)$ is defined to be the contribution from ν number of scatterings to the total multiplicity distribution. In (4.3),

$$\Pi_{\nu,\nu'}(b)=\pi_{\nu}(b)\begin{bmatrix}\nu-1\\ \nu'\end{bmatrix}p^{\nu'}(1-p)^{\nu-1-\nu'} \tag{4.4}$$

and

$$\sigma_{\nu}=\int d^2b\,\pi_{\nu}(b)$$
$$\equiv\int d^2b\frac{[\sigma_{\rm in}^{hN}T(b)]^{\nu}}{\nu!}e^{-\sigma_{\rm in}^{hN}T(b)} \tag{4.5}$$

is the cross section for ν number of scatterings. The total inelastic cross section for an hA collision is then

$$\sigma_{\rm in}^{hA}=\sum_{\nu=1}^{\infty}\sigma_{\nu}=\int d^2b(1-e^{-\sigma_{\rm in}^{hN}T(b)})\ . \tag{4.6}$$

We can see from (4.3) that $P_{n_s}^{s}(\nu)$ is proportional to $\sigma_{\nu}/\sigma_{\rm in}^{hA}$ which is the probability for ν number of collisions. The distribution $Q_{n_s}^{s}(\nu')$ is given by

$$Q_{n_s}^{s}(\nu')=\sum_{m=0}^{\nu'}\binom{\nu'}{m}q^{m}(1-q)^{\nu'-m}Q_{n_s-m-1}(\nu')\ , \tag{4.7}$$

$$Q_{n}(\nu')=\sum_{n_0=0}^{n}P_{n_0}^{hN}F_{n-n_0}^{K'\nu'}(w)\ , \tag{4.8}$$

where P_n^{hN} is the multiplicity distribution of produced particles in hN collisions [see (3.3)] and $F_n^{K'\nu'}(w)$ is the Furry distribution with $K'=\alpha\langle k\rangle_{hN}$ and $\alpha=0.63$ (see Sec. IV of Ref. 1).

From the above equations we can obtain the KNO distribution of shower particles in hA collisions. In the calculation we have used $q=0.5$ and $p=\sigma_{\rm in}^{hN}/\sigma_{\rm in}^{hN}\approx 0.8$. The results are shown in Figs. 11–14 as solid lines for different target nuclei, together with the experimental data from Refs. 8 and 19. With the moments (average

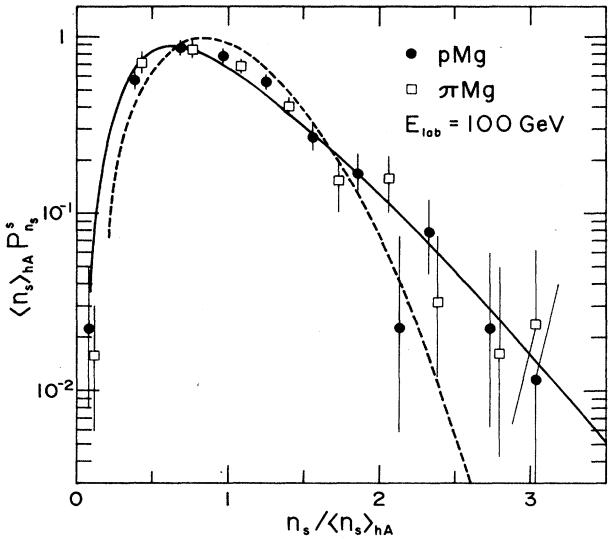

FIG. 11. The KNO plot of multiplicity distribution of shower particles in hMg collisions. The solid line is the calculated results for pMg at $E_{\rm lab}=100$ GeV. The data are from Ref. 8. The dashed line indicates the KNO distribution for pp collisions.

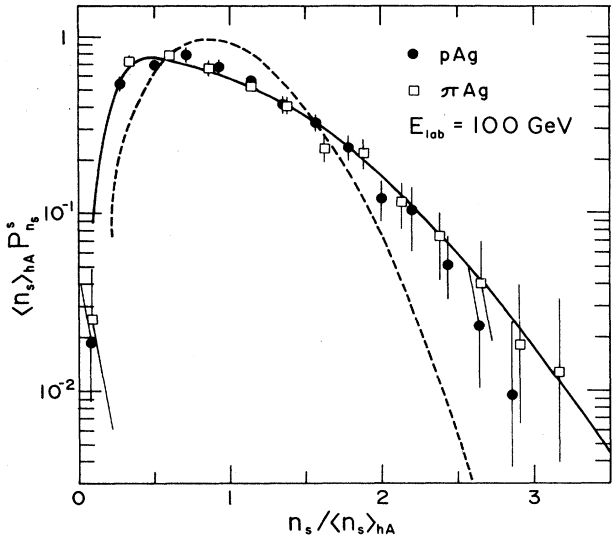

FIG. 13. Same as Fig. 11, except that it is for hAg collisions.

multiplicity, dispersion, and skewness) being so well specified by our model, it is not a surprise that the fitting of our calculated KNO distributions to the data for all types of target nuclei is spectacular. In order to see the A dependence of the KNO distribution ψ^s_{hA}, we also give the distribution ψ^s_{hN} for pp collisions (as dashed lines in Figs. 11–14) which is given by (3.2) and (3.3).

From Figs. 11–14, two properties, which are unique for hA collisions, are observed.

(1) ψ^s_{hA} is always broader than ψ^s_{hN} as expected, due to the multiple scatterings and the fluctuation in their number ν. But what is interesting is that a "shoulder" is building up for heavier nuclei as can be seen clearly in Fig. 13 for Ag and Fig. 14 for Au target.

(2) The position of the peak $z^{(s)\max}_{hA}$ of KNO distribution is shifted to smaller values of $z^{(s)}_{hA}=n_s/\langle n_s\rangle_{hA}$. The heavier the nucleus is, the large the shift or the smaller the value of $z^{(s)\max}_{hA}$ is.

To explain these properties, we plot in Fig. 15 the calculated KNO distribution $\psi^s_{hA}(z^{(s)}_{hA})=\langle n_s\rangle_{hA}\mathcal{P}^s_{n_s}$ for pU collisions (solid line), which is the heaviest target nucleus possible in experiments, and the contributions $\langle n_s\rangle_{hA}P^s_{n_s}(\nu)$, $\nu=1,\ldots,5$, from ν number of scatterings (dot-dashed line). We also show the probability $\sigma_\nu/\sigma^{hA}_{\rm in}$ [see (4.5)] for ν number of scatterings as a function of ν in

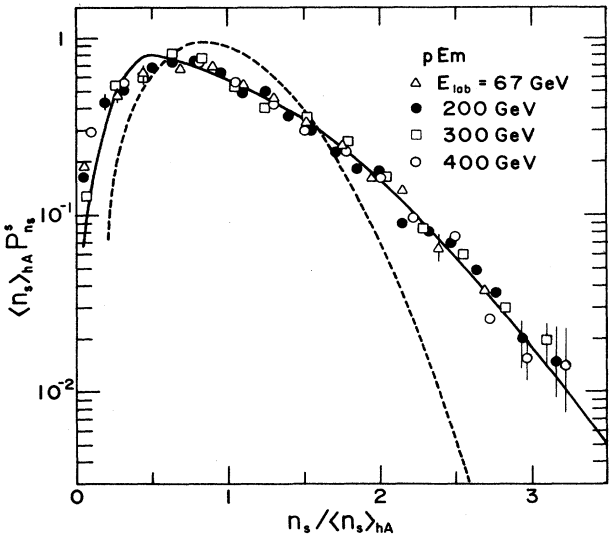

FIG. 12. Same as Fig. 11, except that it is for pEm collision and the data are from Ref. 29.

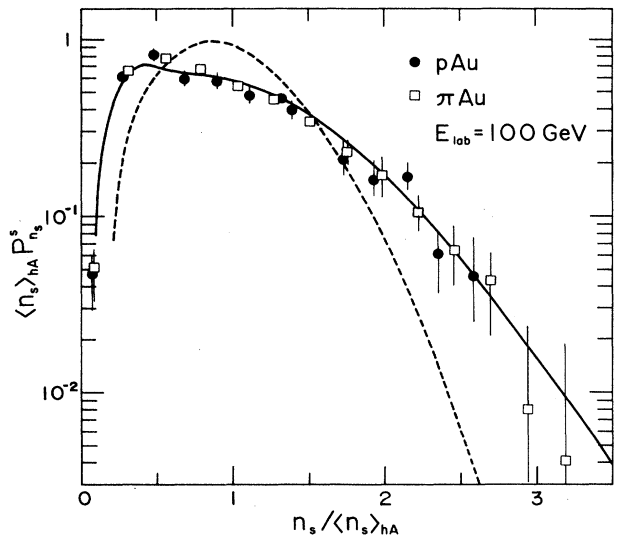

FIG. 14. Same as Fig. 11, except that it is for hAu collisions.

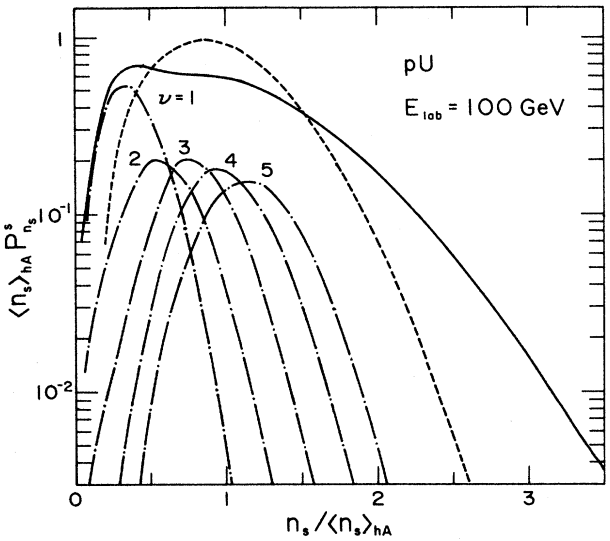

FIG. 15. The calculated KNO distribution for shower particles in pU collisions at $E_{\rm lab}=100$ GeV (solid line). The dot-dashed lines are the contributions to the solid one from events with $\nu=1$, 2, 3, 4, and 5 number of collisions. The dashed line is the KNO distribution for pp collisions.

Fig. 16. We can see that for light nucleus (Mg in Fig. 16, for example), the probability for ν number of scatterings decreases rapidly when $\nu\geq 2$. So are the corresponding contributions to KNO distribution. But when the nucleus becomes heavier (Au in Fig. 16, for example), the values of $\sigma_\nu/\sigma_{\rm in}^{hA}$ for $2\leq\nu\leq 5$ become more comparable

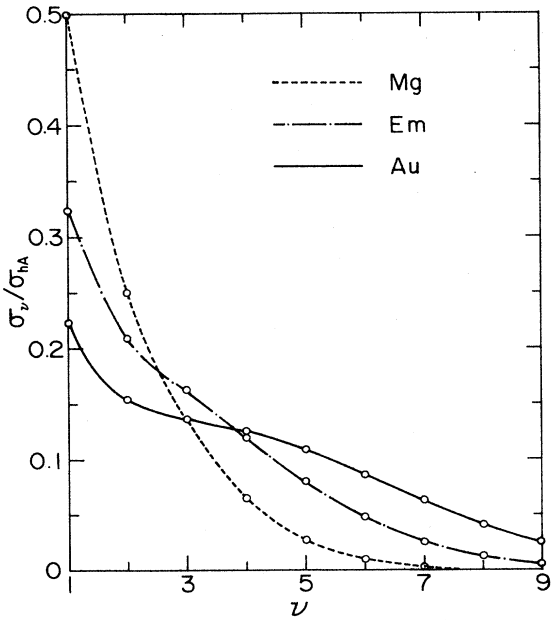

FIG. 16. The normalized cross section $\sigma_\nu/\sigma_{\rm in}^{hA}$ for the events with ν number of collisions as a function of ν. The solid line is for pAu, dot-dashed line for pEm, and dashed line for pMg collision.

to each other. So are the corresponding contributions to total KNO distribution as shown in Fig. 15 for pU collisions. This is how the "shoulder" is building up for heavier nuclei. In Fig. 16, the probability $\sigma_1/\sigma_{\rm in}^{hA}$ is always the largest for each fixed nucleus. Thus the contribution $P^s_{n_s}(\nu=1)$ to $\mathcal{P}^s_{n_s}$ in (4.3) is always dominant among contributions from other values of ν. This is very clear as illustrated in Fig. 15. Therefore, the position of the peak of $\psi^s_{hA}(z^{(s)}_{hA})$ should be approximately determined by $P^s_{n_s}(\nu=1)$. From (4.3)–(4.8), we have

$$P^s_{n_s}(\nu=1)=(\sigma_1/\sigma_{\rm in}^{hA})P^{hN}_{n_s-1}$$
$$=(\sigma_1/\sigma_{\rm in}^{hA})\psi^s_{hN}(z^{(s)}_{hN})/\langle n_s\rangle_{hN}\ , \qquad (4.9)$$

which is just the product of the multiplicity distribution for hN collisions and the probability for h to have only one collisions with a target nucleon. Let the position of the peak of the KNO distribution for hN $\psi^s_{hN}(z^{(s)}_{hN})=\langle n_s\rangle_{hN}P^s_{n_s}$ be $z^{(s)\max}_{hN}$. Then $P^s_{n_s}(\nu=1)$ has its maximum value when

$$n_s\equiv n_1^{\max}=\langle n_s\rangle_{hN} z^{(s)\max}_{hN}\ . \qquad (4.10)$$

The corresponding position of the peak of $\langle n_s\rangle_{hA}P^s_{n_s}(\nu=1)$, when plotted against $z^{(s)}_{hA}=n_s/\langle n_s\rangle_{hA}$, is then

$$z_1^{\max}\equiv n_1^{\max}/\langle n_s\rangle_{hA}$$
$$=(\langle n_s\rangle_{hN}/\langle n_s\rangle_{hA})z^{(s)\max}_{hN}\ . \qquad (4.11)$$

Using (3.1) and (3.6) we have

$$z^{(s)\max}_{hN}/z_1^{\max}=1+\frac{\langle n\rangle_{hN}}{1+\langle n\rangle_{hN}}(\gamma+\beta)(\langle\nu\rangle-1)\ , \qquad (4.12)$$

which is a linear function of $\langle\nu\rangle$. According to our analysis, the position of the peak of $\psi^s_{hA}(z^s_{hA})$ satisfies

$$z^{(s)\max}_{hA}\gtrsim z_1^{\max}\ . \qquad (4.13)$$

As a function of $\langle\nu\rangle$, the calculated $z^{(s)\max}_{hN}/z^{(s)\max}_{hA}$ is plotted in Fig. 17 (solid line), which measures how far the peak of KNO distribution for hA collisions shifts from that for hN collisions. Equation (4.12) is also shown as a dot-dashed line in Fig. 17. By comparing the two curves we can see that (4.13) is indeed true. The difference between $z^{(s)\max}_{hA}$ and $z_1^{\max}$ is due to the contributions from $\langle n_s\rangle_{hN}P^s_{n_s}(\nu)$ for $\nu\geq 2$ to the total KNO distribution $\psi^s_{hA}(z^{(s)}_{hA})$, which makes $z^{(s)\max}_{hA}$ larger than $z_1^{\max}$. For heavier nuclei these contributions become more important and the difference between $z^{(s)\max}_{hA}$ and $z_1^{\max}$ is even larger. In high-energy nucleus-nucleus collisions, the geometrical property of the nucleus becomes more dominant in the problem of multiplicity distribution. Both the shifting of the peak and the building-up of the "shoulder" in KNO multiplicity distribution will be prominent and could not be missed by experimentalists at all.

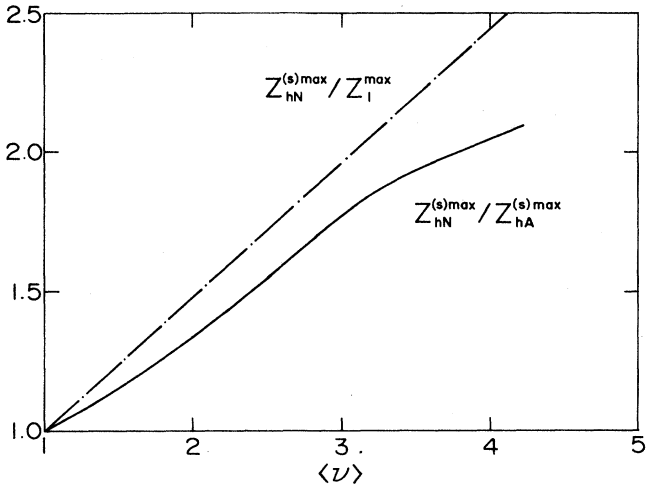

FIG. 17. The calculated $z_{hN}^{(s)max}/z_{hA}^{(s)max}$ (solid line), which measures the shift of the peak of the KNO distribution, as a function $\langle \nu \rangle$. The dashed line obtained from (4.12) measures the shift for the contribution to the KNO curve from events with only $\nu=1$ collision.

V. CONCLUSIONS

We have considered the fluctuations in the number of collisions ν and multiplicity n, using the formula derived in Ref. 1. We have shown that they are closely related. An important result of this study is the demonstration that the measurement of the N_g (number of gray particles) dependence can give a good description of the b dependence. With that connection it is possible to conclude that the multiplicity distributions at various b do not satisfy a universal form. That is based on the theoretical result (which agrees with the experimental data) that the normalized dispersion of the charged multiplicity decreases with increasing N_g.

We then predicted the energy dependence of the multiplicity distribution. For produced particles, the distribution is almost energy independent, due to the scaling property of Furry distribution after smeared over the impact parameter in both hN and hA collisions. The multiplicity distribution for shower particles (or total charged particles in hN case) has a noticeable energy dependence. But for heavier nuclei in hA, this energy dependence is so small that KNO scaling can be considered approximately valid.

We also investigated the A dependence of the multiplicity distribution of shower particles in hA collisions. We found that the fluctuation in multiplicity is larger than in hN collisions, due to the large fluctuation in the number of collisions ν. The dominance of the contribution from the events which have only one hN collision is found to be responsible for the shifting of the peak of KNO distribution to smaller values of $z_{hA}^{(s)}=n_s/\langle n_s \rangle_{hA}$. A shoulder in multiplicity distribution is building up for the large nucleus due to the contributions from the events which have more than one hN collision. With no free parameter to adjust in our calculation, all of these results agree extremely well with the experimental data available. We consider this as a strong support to our consistent treatment to multiplicity distribution in hN and hA collisions and our belief that Furry branching is an important and fundamental process for particle production in soft interactions.

The particle production in hA collisions we have studied in this and the last paper[1] may be called as the *classical* process, where no thermodynamic and hydrodynamic effect is present. In this process, the description of multiple collisions is proved still relevant. An extension of the formalism to nucleus-nucleus collisions thus could be served as a background upon which we could extract some signals of quark-gluon plasma or even a thermalized system if it had ever been formed. We shall discuss this in another paper.

ACKNOWLEDGMENT

This work was supported in part by the U.S. Department of Energy under Grant No. DE-FG06-85ER40224-A001.

APPENDIX

To calculate C_r and $C_r^{(s)}$ we need $\overline{N^r}$ and $\overline{(1+m)^r}$ which are defined as

$$\overline{N^r}(\nu')=\sum_{N=k}^{\infty} N^r F_N^{K'\nu'}(w) , \tag{A1}$$

$$\overline{(1+m)^r}(\nu')=\sum_{m=0}^{\nu'} (m+1)^r B_m(\nu',q) , \tag{A2}$$

where $F_N^{K'\nu'}$ given in (I3.3) and $B_m(\nu',q)$ given in (I2.13) are the Furry and binomial distributions, respectively. By (I3.5), (I3.7), (2.11), and (2.16), we have

$$\overline{N}/\langle n \rangle_{hN}=\alpha\nu' , \tag{A3}$$

$$\overline{N^2}/\langle n \rangle_{hN}^2=\alpha\nu'(a+\alpha)+\alpha^2\nu'(\nu'-1) , \tag{A4}$$

$$\overline{N^3}/\langle n \rangle_{hN}^3=\alpha\nu'[(a+\alpha)(2a+\alpha)+a/\langle n \rangle_{hN}] +3\alpha^2\nu'(\nu'-1)(a+\alpha) +\alpha^3\nu'(\nu'-1)(\nu'-2) , \tag{A5}$$

$$\overline{(1+m)}(\nu')=1+q\nu' , \tag{A6}$$

$$\overline{(1+m)^2}(\nu')=1+3q\nu'+q^2\nu'(\nu'-1) , \tag{A7}$$

$$\overline{(1+m)^3}(\nu')=1+7q\nu'+6q^2\nu'(\nu'-1) +q^3\nu'(\nu'-1)(\nu'-2) . \tag{A8}$$

Then for produced particles we can obtain, from (I3.9) and (2.13),

$$\overline{n}(\nu')/\langle n \rangle_{hN}=1+\alpha\nu' , \tag{A9}$$

$$\overline{n^2}(\nu')/\langle n \rangle_{hN}^2=C_2^{hN}+\alpha\nu'(2+\alpha+a)+\alpha^2\nu'(\nu'-1) , \tag{A10}$$

$$\overline{n^3}(\nu')/\langle n \rangle_{hN}^3=C_3^{hN}+\alpha\nu'[3C_2^{hN}+(\alpha+a)(3+2a+\alpha)+a/\langle n \rangle_{hN}]+3\alpha^2\nu'(\nu'-1)(1+a+\alpha)+\alpha^3\nu'(\nu'-1)(\nu'-2) . \tag{A11}$$

For shower particle we use (2.18) to calculate $\overline{n_s^r}(\nu')$, and then get

$$\bar{n}_s(\nu')=1+q\nu'+\bar{n}(\nu') , \tag{A12}$$

$$\overline{n_s^2}(\nu')=\overline{(1+m)^2}(\nu')+2\langle n\rangle_{hN}d_{21}(\nu')+\overline{n^2}(\nu') , \tag{A13}$$

$$\overline{n_s^3}(\nu')=\overline{(1+m)^3}(\nu')+3\langle n\rangle_{hN}d_{31}(\nu')+3\langle n\rangle_{hN}^2 d_{32}(\nu')+\overline{n^3}(\nu') , \tag{A14}$$

with $d_{21}(\nu')$, $d_{31}(\nu')$, and $d_{32}(\nu')$ given by

$$d_{21}(\nu')=1+(q+\alpha+q\alpha)\nu'+q\alpha\nu'(\nu'-1) , \tag{A15}$$

$$d_{31}(\nu')=1+\nu'(3q+\alpha+3q\alpha)+\nu'(\nu'-1)(q^2+3q\alpha+2q^2\alpha)+q^2\alpha\nu'(\nu'-1)(\nu'-2) , \tag{A16}$$

$$\begin{aligned} d_{32}(\nu')=&C_2^{hN}+\nu'[(2+\alpha+a)\alpha+qC_2^{hN}+(2+\alpha+a)q\alpha]+\nu'(\nu'-1)[\alpha^2+(2+\alpha+a)q\alpha+2q\alpha^2] \\ &+q\alpha^2\nu'(\nu'-1)(\nu'-2) . \end{aligned} \tag{A17}$$

Because of (I3.11), (I3.12), (I3.13), and (2.16) with $\beta=\alpha p$ the average over ν' and ν yields

$$\langle n\rangle_{hA}(\tilde{\nu})/\langle n\rangle_{hN}=1+\beta(\tilde{\nu}-1) , \tag{A18}$$

$$\langle n^2\rangle_{hA}(\tilde{\nu})/\langle n\rangle_{hN}^2=C_2^{hN}+\beta(\tilde{\nu}-1)(2+\alpha+a-2\beta)+\beta^2\langle\nu(\nu-1)\rangle\tilde{} , \tag{A19}$$

$$\begin{aligned} \langle n^3\rangle_{hA}(\tilde{\nu})/\langle n\rangle_{hN}^3=&C_3^{hN}+\beta(\tilde{\nu}-1)[3C_2^{hN}+(a+\alpha)(3+\alpha+2a-6\beta)-6\beta(1-\beta)+a/\langle n\rangle_{hN}] \\ &+3\beta^2\langle\nu(\nu-1)\rangle\tilde{}(1+\alpha+a-\beta)+\beta^3\langle\nu(\nu-1)(\nu-2)\rangle\tilde{} , \end{aligned} \tag{A20}$$

and, with $\gamma=pq$,

$$\langle n_s\rangle_{hA}(\tilde{\nu})=1+\gamma(\tilde{\nu}-1)+\langle n\rangle_{hA}(\tilde{\nu}) , \tag{A21}$$

$$\langle n_s^2\rangle_{hA}(\tilde{\nu})=\langle(1+m)^2\rangle(\tilde{\nu})+2\langle n\rangle_{hN}\langle d_{21}\rangle(\tilde{\nu})+\langle n^2\rangle_{hA}(\tilde{\nu}) , \tag{A22}$$

$$\langle n_s^3\rangle_{hA}(\tilde{\nu})=\langle(1+m)^3\rangle(\tilde{\nu})+3\langle n\rangle_{hN}\langle d_{31}\rangle(\tilde{\nu})+3\langle n\rangle_{hN}^2\langle d_{32}\rangle(\tilde{\nu})+\langle n^3\rangle_{hA}(\tilde{\nu}) , \tag{A23}$$

where

$$\langle(1+m)^2\rangle(\tilde{\nu})=1+\gamma(3-2\gamma)(\tilde{\nu}-1)+\gamma^2\langle\nu(\nu-1)\rangle\tilde{} , \tag{A24}$$

$$\langle(1+m)^3\rangle(\tilde{\nu})=1+(7-12\gamma+6\gamma^2)\gamma(\tilde{\nu}-1)+(6-3\gamma)\gamma^2\langle\nu(\nu-1)\rangle\tilde{}+\gamma^3\langle\nu(\nu-1)(\nu-2)\rangle\tilde{} , \tag{A25}$$

$$\langle d_{21}\rangle(\tilde{\nu})=1+(\tilde{\nu}-1)(\gamma+\beta+q\beta-2\gamma\beta)+\gamma\beta\langle\nu(\nu-1)\rangle\tilde{} , \tag{A26}$$

$$\begin{aligned} \langle d_{31}\rangle(\tilde{\nu})=&1+(\tilde{\nu}-1)[\beta+3\gamma(1+\alpha-2\beta)-2\gamma^2(1+2\alpha-3\beta)] \\ &+\langle\nu(\nu-1)\rangle\tilde{}\gamma[3\beta+\gamma(1+2\alpha-3\beta)]+\beta\gamma^2\langle\nu(\nu-1)(\nu-2)\rangle\tilde{} , \end{aligned} \tag{A27}$$

$$\begin{aligned} \langle d_{32}\rangle(\tilde{\nu})=&C_2^{hN}+(\tilde{\nu}-1)[\gamma C_2^{hN}+(2+\alpha+a)\beta(1+q-2\gamma)-2\beta^2(1+2q-3\gamma)] \\ &+\langle\nu(\nu-1)\rangle\tilde{}\beta[\gamma(2+\alpha+a)]+\beta(1+2q-3\gamma)+\gamma\beta^2\langle\nu(\nu-1)(\nu-2)\rangle\tilde{} . \end{aligned} \tag{A28}$$

In the above equations $\langle\cdots\rangle\tilde{}$ denotes the averages of the types (2.1), (2.3), or (2.4) according to what $\tilde{\nu}$ is.

From (A18)–(A28) we can immediately calculate the moments $C_r=\langle n^r\rangle_{hA}/\langle n\rangle_{hA}^r$, $C_r^{(s)}=\langle n_s^r\rangle_{hA}/\langle n_s\rangle_{hA}^r$, and their dependences on $\tilde{\nu}$.

[1] R. C. Hwa and X.-N. Wang, preceding paper, Phys. Rev. D **39**, 2561 (1989).

[2] W. H. Furry, Phys. Rev. **52**, 569 (1937); N. Arley, *Stochastic Processes and Cosmic Radiation* (Wiley, New York, 1948), p. 92.

[3] W. R. Chen, R. C. Hwa, and X.-N. Wang, Phys. Rev. D **38**, 3394 (1988).

[4] W. R. Chen and R. C. Hwa, Phys. Rev. D **36**, 760 (1987).

[5] D. Kiang, S. H. Ling, K. Young, and C. S. Lam, Phys. Rev. D **31**, 31 (1985).

[6] W. Thomé *et al.*, Nucl. Phys. **B129**, 365 (1977).

[7] R. Szwed, G. Wrochna, and A. K. Wroblewski, Acta Phys. Pol. B **19**, 763 (1988).

[8] N. N. Biswas *et al.*, Phys. Rev. D **33**, 3167 (1986).

[9] See R. C. Hwa, in *Hadronic Multiparticle Production*, edited by P. Carruthers (World Scientific, Singapore, 1988), p. 556.

[10] R. Møller, Nucl. Phys. **B74**, 145 (1974).

[11] P. Carruthers and C. C. Shih, Phys. Lett. **127B**, 242 (1983).

[12] C. De Marzo *et al.*, Phys. Rev. D **26**, 1019 (1982).

[13] A. Wroblewski, Acta Phys. Pol. B **4**, 857 (1973).

[14]Reference 7 has an extensive list of the references on the experimental data.
[15]W. R. Chen and R. C. Hwa, Phys. Rev. D **39**, 179 (1989).
[16]L. Jones *et al.*, Phys. Rev. Lett. **33**, 1440 (1974); A. Carroll *et al.*, Phys. Lett. **80B**, 319 (1979).
[17]L. Durand and H. Pi, Phys. Rev. D **38**, 78 (1988).
[18]J. Babecki *et al.*, Phys. Lett. **47B**, 268 (1973).
[19]I. Otterlund *et al.*, Nucl. Phys. **B142**, 445 (1978).